ACS APPLIED MATERIALS & INTERFACES

Research Article

www.acsami.org

Generating Electric Current Based on the Solvent-Dependent Charging Effects of Defective Boron Nitride Nanosheets

Ronghui Que,*[,†] Yucheng Huang,[†] Qinling Li,[‡] Hong Yao,[†] Baoyou Geng,*[,†] and Mingwang Shao*[,‡]

[†]Anhui Laboratory of Molecule-Based Materials, Anhui Key Laboratory of Chemo-Biosensing, The Key Laboratory of Functional Molecular Solids, Ministry of Education College of Chemistry and Materials Science, Anhui Normal University, Wuhu 241000, China

[‡]Institute of Functional Nano and Soft Materials (FUNSOM) and Jiangsu Key Laboratory for Carbon-based Functional Materials and Devices, Soochow University, Suzhou, Jiangsu 215123, P. R. China

Supporting Information

ABSTRACT: This work presents a method of generating electric current based on the defects of few-layer boron nitride nanosheets (BNNSs). The density functional theory calculations showed that the atomic charge of the B atom in acetone was more positive than in water. The electrostatic force microscopy measurements illustrated that the local electrical potential was 0.35 mV in acetone, while the potential signal was very difficult to capture when using water as the dispersant. This effect was further demonstrated by the performance of the acoustic energy-harvesting nanogenerator: the BNNSs were assembled into a film after being dispersed in acetone and then integrated into the generator device, generating average output current of ∼0.98 nA, which was much better than 0.2 nA, the average output current of another device with water as the dispersant. These results demonstrated that solvent effects made the as-prepared BNNSs carry net charges, which could be utilized to harvest acoustic energy and generate current.

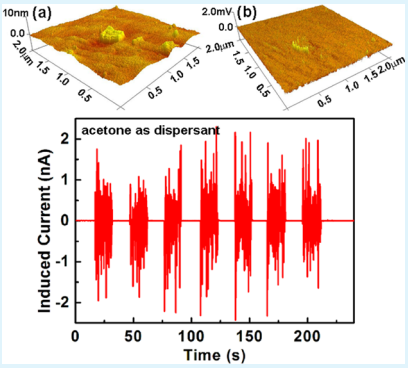

KEYWORDS: *boron nitride nanosheets, defects, solvent effect, acoustic energy*

INTRODUCTION

Generating electricity based on the two-dimensional graphene is the hot spot in the field of graphene research.[1,2] Sheets of hexagonal boron nitride (*h*-BN) are composed of alternating boron and nitrogen atoms in a two-dimensional honeycomb lattice consisting of sp^2 bonds. Because of its structural similarity to graphene[3] and its interesting properties, such as exceptional mechanical and thermal properties, chemical stability,[4] and UV emission,[5] monolayer *h*-BN has attracted a great deal of attention. The pristine BN sheets are intrinsically insulators or wide band gap semiconductors (approximately 5.6 eV).[6] Because of its good electrical insulation, *h*-BN has been extensively applied as a charge linkage layer in many electronic devices.[3,7−9]

The prerequisite for such applications is the mass production of *h*-BN sheets in a controlled manner with perfect structure. To date, only the expensive methods of chemical vapor deposition (CVD)[10−15] and unwrapping nanotubes with plasma etching[16] can meet the criterion of electronic devices.[7] The more important issue is the limited yields of these methods, not to mention the extensive applications. The few-layer *h*-BN from those convenient and large-scale synthesis methods, such as liquid exfoliation,[17−19] chemical synthesis,[20,21] and traditional mechanical exfoliation,[22] is difficult to use in devices because of the existence of impurities or defects.

However, vacancies, adatoms, and topological defects are inevitable in reality, which may significantly impact the electronic properties and chemical reactivity of nanomaterials. To fully utilize the large amount of BN nanosheets (BNNSs) with impurities and defects, the charge distribution of BNNSs in different dispersants was computed with the density functional theory (DFT) method and the local electrical potentials in acetone and water were measured using electrostatic force microscopy (EFM). Both results indicated the nanosheets dispersed in acetone carried many more charges than in water. They were assembled into a film and integrated in a nanogenerator, which was similar to the method reported previously.[23,24] The nanogenerator generated an average output current of 0.98 nA. By contrast, the output current greatly decreased when water was used as the dispersant.

EXPERIMENTAL SECTION

Synthesis of BNNSs. The synthesis method of BNNSs is similar to that described in the literature,[20] and the schematic is shown in Figure S1 of the Supporting Information. Briefly, a mixture of boric acid (AR, Aldrich) and urea (AR, Aldrich) with a molar ratio of 1:48 was dissolved in 40 mL of distilled water and heated at 65 °C until the water had completely evaporated. The mixture precursor in an alumina boat was placed at the center of a horizontal alumina tube mounted inside a high-temperature tube furnace. The system was slowly evacuated to a base pressure of 100 Pa. The furnace was heated to 900 °C at a rate of 80 °C/min and kept at this temperature for 5 h in a N_2 atmosphere. The white products were collected in the alumina boat.

Received: July 23, 2014
Accepted: November 5, 2014
Published: November 5, 2014

The exfoliated BNNSs were prepared from *h*-BN microsized particles using the method described in the literature.[18] In the experiment, BN powder (0.5 g, AR, Aldrich) in *N*,*N*-dimethylformamide (DMF) (30 mL) was strongly sonicated for 12 h and then centrifuged at 8000 rpm to remove the residual large BN particles. The solution was dried, and the collected products were washed several times with ethanol.

Instruments. The crystal structure of the samples was characterized by X-ray powder diffraction (XRD) by using an X'Pert-ProMPD (Holand) D/max-γAX-ray diffractometer with Cu Kα radiation (λ = 0.15406 nm) and transmission electron microscopy (TEM) (FEI Tecnai F20, 200 kV). Raman spectra were recorded using a confocal microprobe Raman system (HR800, Jobin Yvon) using a 633 nm HeNe laser. The electronic structure of carbon was characterized via X-ray photoemission spectroscopy (XPS) (Kratos Axis UltraDLD, monochromatized Al Kα source) operated at a base pressure of 5×10^{-10} Torr. Atomic force microscopy (AFM) measurements were conducted with a Mutilmode V AFM system (Veeco) using tapping mode. Fourier transform infrared (FTIR) measurements were performed in air using a Bruker FTIR spectrometer.

Computational Methods. All the calculations were conducted within the framework of Gaussian 09. The effects of solvent on geometry and charge distribution were considered using the polarized continuum (PCM) model. Two experimentally used solvents, water and acetone, were taken into account. Ground state optimizations of the BN sheet in solution have been performed by using the B3LYP hybrid function with the 6-31G(d) basis set at a DFT level. Here, the BN sheet is modeled as a finite structure (Figure 4), where a B-rich pentagon−heptagon (5|7) pair is introduced. Test calculations show that the structures with heteroelemental bonds in a pristine BN sheet and square−octagon (4|8) pairs as well as the N-rich 5|7 pairs are either electroneutral or negatively charged, which contradict the results of our EFM experiment. Furthermore, the edged unsaturated B atoms are terminated with O according to XPS evidence, and other edged atoms are all passivated by H atoms.

RESULTS AND DISCUSSION

Characterization of BNNSs and the Existence of Defects. The transmission electron microscopy (TEM) image in Figure 1a shows the sheetlike nanostructure of the as-prepared BN with wrinkles in the center, making it easier to distinguish the presence of sheets and the typical layered compound. The high-resolution TEM image in Figure 1b displays the interlayer (002) lattice fringe (0.35 nm) of layered BN, which is consistent with the previous reports.[18,25] The appearance of some arches (green arrows) and amorphous areas (red circles) demonstrates the existence of some disorders due to the defects and impurities.[26]

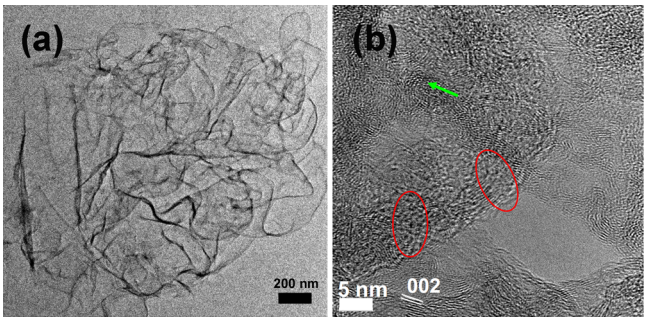

Figure 1. (a) TEM image of the products. (b) high-resolution TEM image of h-BN. The green arrow denotes the arches, and the red circles are the amorphous areas.

The X-ray diffraction (XRD) profile of the BNNSs is shown Figure S2 of the Supporting Information. All the peaks can be assigned to those of *h*-BN (JCPDS Card 45-0896), which strongly agree with those described in the literature.[5] Note that the decrease in (002) peak intensity might be indicative of the increase in the level of *h*-BN disorder or defect density.[27] The typical Raman spectra taken from the BNNSs (Figure 2a, red curve) and a bulk *h*-BN (black curve) show a dominant peak near 1370 cm^{-1}, which can be attributed to the B−N vibrational mode (E_{2g}) within *h*-BN layers,[28] further confirming the hexagonal structure of the prepared BNNSs. The band of BNNSs shifts to a higher frequency, and the full width at half-maxima (fwhm) obviously broadens compared with that of bulk *h*-BN, suggesting the few-layer structure of BNNSs[29] and the increased degree of oxidation.[30]

To further investigate the local structure of the as-obtained materials, the chemical states of B and C elements were investigated using X-ray photoelectron spectrometry (XPS) spectra. Panels c and d of Figure 2 show the typical B 1s and N 1s spectra, respectively. The observed binding energy of B 1s from the XPS measurement is 190.5 eV, which is very close to that in the *h*-BN bulk phase (190.1 eV).[23] The N 1s peak is located at 397.8 eV, in good agreement with the reported position of the N 1s spectrum (398.1 eV) of *h*-BN.[13] The shoulder at 192.1 eV in the B 1s spectrum is assigned to the structure-terminating B−O bonds,[25] while the shoulder at 399.2 eV in the N 1s spectrum may be from the N−C bonds,[31] which may originate from the few precursor residues. Both these shoulders are observed through the weak vibrations at 1198 and 1630 cm^{-1} in the FTIR spectrum (Figure 2b), respectively, which are in good agreement with values from the previous report.[25] The two strong bands at 800 and 1396 cm^{-1} (Figure 2b) are assigned to the in-plane stretching and out-of-plane bending vibrations of *h*-BN, respectively.[25] Taken together, the XPS analysis, the HRTEM structural characterization, the Raman spectrum, and the FTIR vibrational analysis all support the fact that the as-prepared BNNSs are defective.

Characterization of the Local Potential of BNNNs. More interestingly, the existence of the defects makes the BNNSs carry net charges, as evidenced by electrostatic force microscopy (EFM) characterization. In our experiment, the surface topography and local charge distribution on the BNNSs at the same position were concurrently monitored. Figure 3 presents the AFM three-dimensional (3D) images of the BNNSs' topography and corresponding electrostatic force measured at room temperature in air. As seen in Figure 3a, the bright regions correspond to the height of the BNNS, and the corresponding line-scan profile in Figure 3c indicates a thickness of ~3 nm, demonstrating the formation of few-layer *h*-BN.[12,25]

The obvious bright and dark segments in the EFM image (Figure 3b) correspond to the presence of positive and negative charges on BNNSs, respectively. The 3D image convincingly shows that the BNNS is mainly positively charged, and the line-scan profile in Figure 3d indicates the surface positive potential is 0.35 mV. However, in water, the surface positive potential of the BNNSs is ~0.09 mV (Figure S3b of the Supporting Information), which is almost too small to be captured.

Theoretical Support of Surface Potential. As a further support, the DFT calculations were used to validate the presence of net charge. The literature had reported that only the B-rich pentagon−heptagon pairs (5|7s) were positive,[32] so the Stone−Wales defects were selected without considering

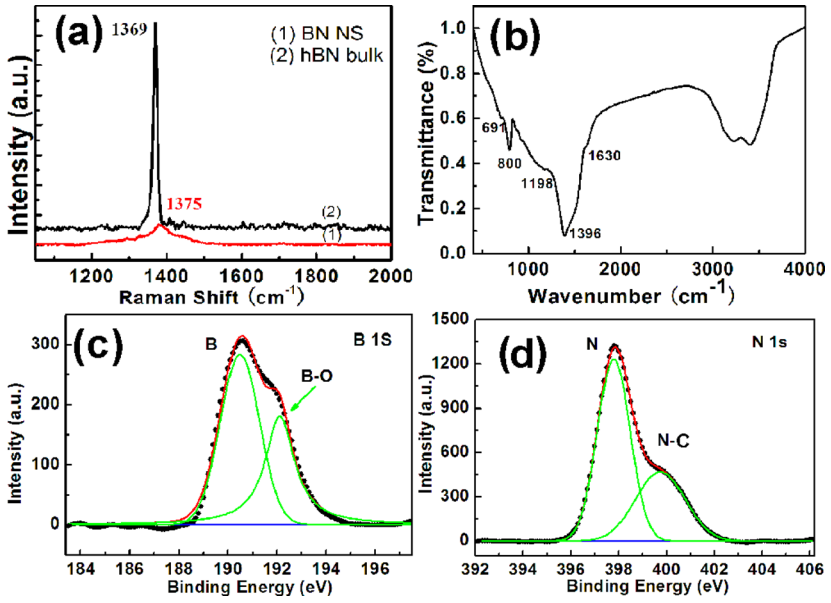

Figure 2. (a) Raman spectra of BNNSs and bulk *h*-BN. (b) FTIR spectrum of BNNSs. (c and d) XPS spectra of B 1s and N 1s, respectively.

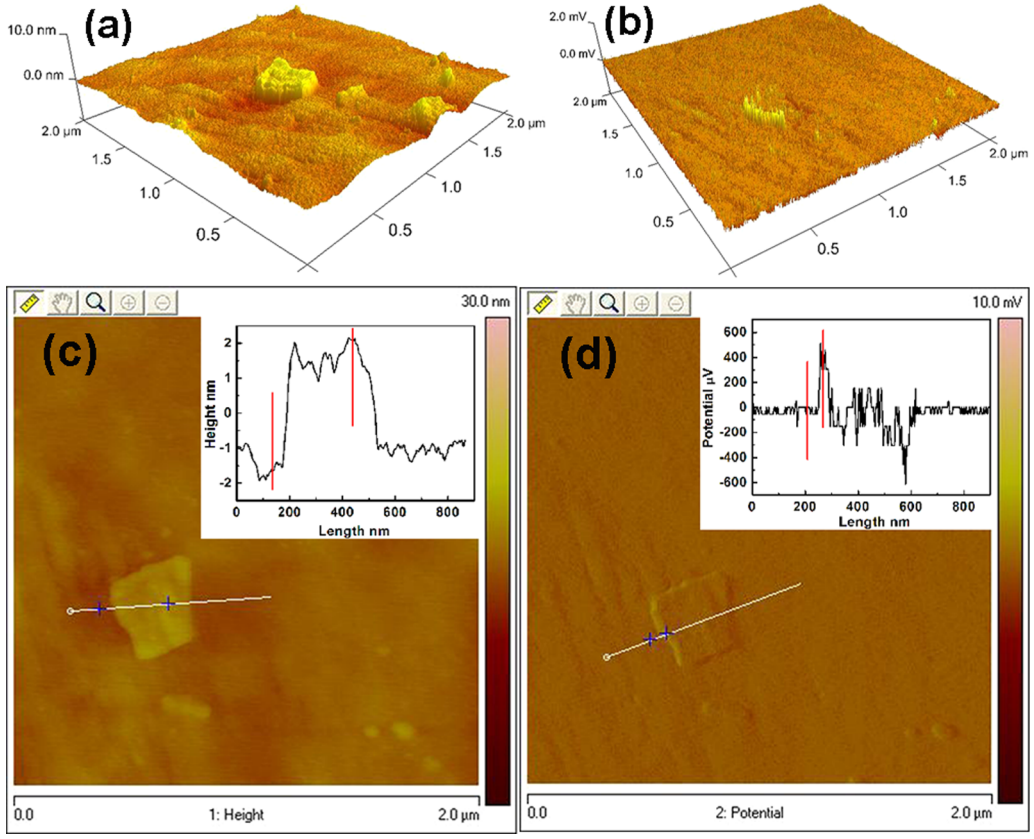

Figure 3. 3D images of (a) topography and (b) simultaneously recorded electrostatic forces (image size, 2 μm × 2 μm). (c) AFM image of the BNNSs and the corresponding line-scan profile. (d) EFM image of the BNNSs and the corresponding line-scan profile.

other defects. As labeled in Figure 4, the calculated Mülliken charge populations clearly demonstrate that the B-rich pentagon−heptagon (5|7) pair is indeed positively charged, which is in accordance with the EFM results. Moreover, from water to acetone, the atomic charge of the B atom increases ~0.01−0.02 per atom, while the charge of N essentially remains unchanged.

Fabrication of the Generator Device. To utilize the net charges from the defects, a generator device based on the charged BNNSs was fabricated. Figure 5 sketches the fabrication process of the BNNS film device. BNNSs (0.02 g) were added to acetone (2 mL) and sonicated for 5−8 min to form a dispersed suspension. This suspension (200 μL) was dropped onto a Teflon tape and dried under an ambient atmosphere for ~10 min to form a BNNS film (Figure S4 of

dx.doi.org/10.1021/am504777g | ACS Appl. Mater. Interfaces 2014, 6, 19752−19757

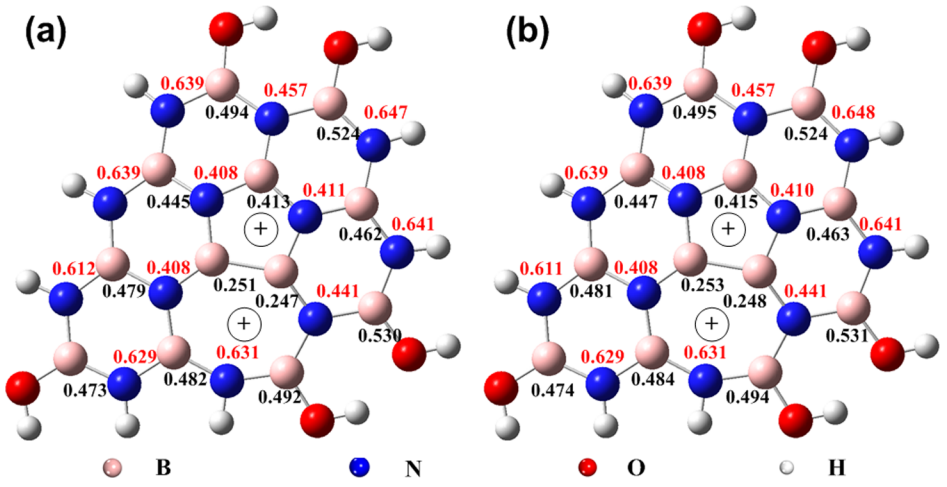

Figure 4. Mülliken charge populations of the BN sheet in (a) water and (b) acetone. Numbers in red denote negative charges.

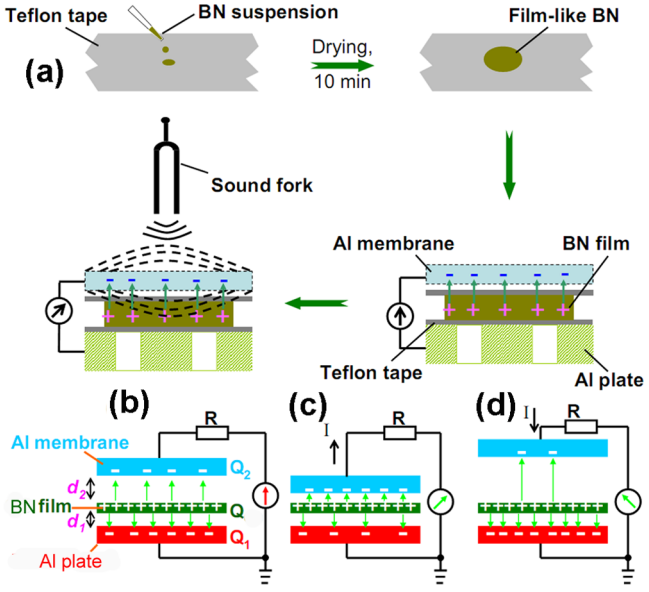

Figure 5. (a) Schematic of the experimental setup of the generator with BNNSs. (b–d) Equivalent circuits of current generation.

the Supporting Information). The film was assembled into an energy harvester as shown in Figure 5a. This structure consisted of only one movable part, which may yield sustainable and stable output currents.[23] The detailed fabrication of the energy-harvesting generator is described in the Supporting Information, and the working mechanism of the generator has been extensively described in our previous reports.[23,24]

The net charges on the film can be explained as follows. The BN nanosheets are excellent dielectric materials, and the solvents make the defects of BNNS charged or polarized under heating. With the evaporation of the solvents, the polarization remains frozen after cooling, which is similar to the formation of inorganic electrets.[33] Therefore, the dried BNNS film acts as an "electret" that can carry net charges.

Systematic Study of the Performance of the Generator Device. Briefly, the equivalent circuit of the BNNS-based generator is illustrated in Figure 5b–d, in which the device can be regarded as a flat-panel capacitor with a capacitance $C = \varepsilon S/d$, where ε is the spacer dielectric constant, S is the effective capacitor area, and d is the interspacing distance. When the sound fork is stationary, the Al membrane remains steady (Figure 5b), in which the induced counter charge quantity (Q) follows the relationship $CV_0 = Q$. In this case, only the background noise current (~3.2 pA) can be detected. When the sound fork is vibrating, the Al membrane would responsively vibrate, resulting in a transient current as schematically depicted in Figure 5c and vice versa, as depicted in Figure 5d. A continuous alternating current could therefore be generated in the circuit as shown in Figure 6a. The average

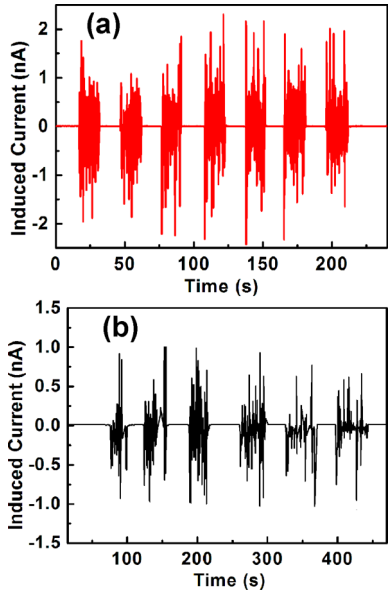

Figure 6. Induced current of the nanogenerator vs vibration of a sound fork: (a) actone as the dispersant and (b) water as the dispersant.

absolute current is ~0.98 nA (Figure 6a) with a large signal-to-noise ratio of >360. In contrast, no current response was observed in the reference device with the exfoliated BNNSs (Figure S5 of the Supporting Information) and without BNNSs (Figure S6 of the Supporting Information) using the identical device structure, indicating the charged film of BNNSs is responsible for current generation.

A control experiment was conducted with another BNNS film, which was made using water as the dispersant instead of the acetone, and assembled into the identical device structure.

dx.doi.org/10.1021/am504777g | ACS Appl. Mater. Interfaces 2014, 6, 19752–19757

The measured maximal current is ~0.85 nA (Figure 6b), and the average value is 0.2 nA, which decreases greatly and less strongly than the former average value. The large decrease in output current indicates the decrease in charges in the BNNS film according to the working mechanism of the generator. It is also the most important reason why the output current of the BNNS-based generator is lower than the values in our previous reports. Nevertheless, these results are enough to confirm the fact that the existence of defects results in the solvents effects of BNNSs and can be made to generate electric current.

CONCLUSIONS

In summary, BNNSs from the chemical method are charged because of the existence of defects. The charged BNNS films can be conveniently integrated into generators for harvesting acoustic energy. The dispersant of BNNSs greatly affected the local electrical potential and the performance of the device. The average output current of the device with BNNSs dispersed in acetone is 0.98 nA, which is almost 5 times higher than that of BNNSs dispersed in water due to the charge distribution. As the defective BNNSs are inexpensive and easily processed, the BNNS-based generator will open up a novel application for BNNSs.

ASSOCIATED CONTENT

Supporting Information

Schematic illustration of the synthesis process, XRD pattern of BNNSs, and the fabrication of the generator. This material is available free of charge via the Internet at http://pubs.acs.org.

AUTHOR INFORMATION

Corresponding Authors

*E-mail: mwshao@suda.edu.cn.
*E-mail: qrhui123@mail.ahnu.edu.cn.
*E-mail: bygeng@mail.ahnu.edu.cn.

Notes

The authors declare no competing financial interest.

ACKNOWLEDGMENTS

This work was supported by the National Natural Science Foundation of China (Grant 21301006), the Specialized Research Fund for the Doctoral Program of Higher Education (Grant 20133424120003), and the Anhui Natural Science Foundation (Grant 1308085QB32). The reviewers' invaluable comments are greatly appreciated.

REFERENCES

(1) Yin, J.; Li, X.; Yu, J.; Zhang, Z.; Zhou, J.; Guo, W. Generating Electricity by Moving a Droplet of Ionic Liquid along Graphene. *Nat. Nanotechnol.* **2014**, *9*, 378−383.
(2) Yin, J.; Zhang, Z.; Li, X.; Yu, J.; Zhou, J.; Chen, Y.; Guo, W. Waving Potential in Graphene. *Nat. Commun.* **2014**, *5*, 3582−3587.
(3) Levendorf, M. P.; Kim, C. J.; Brown, L.; Huang, P. Y.; Havener, R. W.; Muller, D. A.; Park, J. Graphene and Boron Nitride Lateral Heterostructures for Atomically Thin Circuitry. *Nature* **2012**, *488*, 627−632.
(4) Chen, Y.; Zou, J.; Campbell, S. J.; Le, C. G. Boron Nitride Nanotubes: Pronounced Resistance to Oxidation. *Appl. Phys. Lett.* **2004**, *84*, 2430−2432.
(5) Kubota, Y.; Watanabe, K.; Tsuda, O.; Taniguchi, T. Deep Ultraviolet Light-Emitting Hexagonal Boron Nitride Synthesized at Atmospheric Pressure. *Science* **2007**, *317*, 932−934.
(6) Song, L.; Liu, Z.; Reddy, A. L. M.; Narayanan, N. T.; Jaime, T. T.; Peng, J.; Gao, G.; Lou, J.; Robert, V.; Pulickel, M. A. Binary and Ternary Atomic Layers Built from Carbon, Boron, and Nitrogen. *Adv. Mater.* **2012**, *24*, 4878−4895.
(7) Garcia, A. G. F.; Neumann, M.; Amet, F.; Williams, J. R.; Watanabe, K.; Taniguchi, T.; Gordon, D. G. Effective Cleaning of Hexagonal Boron Nitride for Graphene Devices. *Nano Lett.* **2012**, *12*, 4449−4454.
(8) Watanabe, K.; Taniguchi, T.; Niiyama, T.; Miya, K.; Taniguchi, M. Far-ultraviolet Plane-Emission Handheld Device Based on Hexagonal Boron Nitride. *Nat. Photonics* **2009**, *3*, 591−594.
(9) Dean, C. R.; Young, A. F.; Meric, I.; Lee, C.; Wang, L.; Sorgenfrei, S.; Watanabe, K.; Taniguchi, T.; Kim, P.; Shepard, K. L.; Hone, J. Boron Nitride Substrates for High-Quality Graphene Electronics. *Nat. Nanotechnol.* **2010**, *5*, 722−726.
(10) Sachdev, H.; Mueller, F.; Huefner, S. Formation of Boron-Based Films and Boron Nitride Layers by CVD of a Boron Ester. *Angew. Chem., Int. Ed.* **2011**, *50*, 3701−3705.
(11) Lee, K. H.; Shin, H. J.; Lee, J.; Lee, I.; Kim, G. H.; Choi, J. Y.; Kim, S. W. Large-Scale Synthesis of High-Quality Hexagonal Boron Nitride Nanosheets for Large-Area Graphene Electronics. *Nano Lett.* **2012**, *12*, 714−718.
(12) Kim, K. K.; Hsu, A.; Jia, X. T.; Kim, S. M.; Shi, Y.; Hofmann, M.; Nezich, D.; Rodriguez-Nieva, J. F.; Dresselhaus, M.; Palacios, T.; Kong, J. Synthesis of Monolayer Hexagonal Boron Nitride on Cu Foil Using Chemical Vapor Deposition. *Nano Lett.* **2012**, *12*, 161−166.
(13) Shi, Y. M.; Hamsen, C.; Jia, X. T.; Kim, K. K.; Reina, A.; Hofmann, M.; Hsu, A. L.; Zhang, K.; Li, H. N.; Juang, Z. Y. Synthesis of Few-Layer Hexagonal Boron Nitride Thin Film by Chemical Vapor Deposition. *Nano Lett.* **2010**, *10*, 4134−4139.
(14) Yin, J.; Li, X.; Zhou, J.; Guo, W. Ultralight Three-Dimensional Boron Nitride Foam with Ultralow Permittivity and Superelasticity. *Nano Lett.* **2013**, *13*, 3232−3236.
(15) Li, X.; Yin, J.; Zhou, J.; Guo, W. Large Area Hexagonal Boron Nitride Monolayer as Efficient Atomically Thick Insulating Coating against Friction and Oxidation. *Nanotechnology* **2014**, *25*, 105701−105706.
(16) Zeng, H.; Zhi, C.; Zhang, Z.; Wei, X.; Wang, X.; Guo, W.; Bando, Y.; Golberg, D. "White Graphenes": Boron Nitride Nanoribbons via Boron Nitride Nanotube Unwrapping. *Nano Lett.* **2010**, *10*, 5049−5055.
(17) Lin, Y.; Williams, T. V.; Connell, J. W. Soluble, Exfoliated Hexagonal Boron Nitride Nanosheets. *J. Phys. Chem. Lett.* **2010**, *1*, 277−283.
(18) Zhi, C.; Bando, Y.; Tang, C.; Kuwahara, H.; Golberg, D. Large-Scale Fabrication of Boron Nitride Nanosheets and Their Utilization in Polymeric Composites with Improved Thermal and Mechanical Properties. *Adv. Mater.* **2009**, *21*, 2889−2893.
(19) Li, C.; Bando, Y.; Zhi, C.; Huang, Y.; Golberg, D. Thickness-Dependent Bending Modulus of Hexagonal Boron Nitride Nanosheets. *Nanotechnology* **2009**, *20*, 385707−358713.
(20) Angshuman, N.; Kalyan, R.; Kailash, P. S. S. H.; Ranjan, D.; Umesh, V. W.; Rao, C. N. R. Graphene Analogues of BN: Novel Synthesis and Properties. *ACS Nano* **2010**, *4*, 1539−1544.
(21) Wang, X.; Zhi, C.; Li, L.; Zeng, H.; Li, C.; Mitome, M.; Golberg, D.; Bando, Y. "Chemical Blowing" of Thin-Walled Bubbles: High-Throughput Fabrication of Large-Area, Few-Layered BN and Cx-BN Nanosheets. *Adv. Mater.* **2011**, *23*, 4072−4076.
(22) Pacile, D.; Meyer, J. C.; Girit, C. O.; Zettl, A. The Two-Dimensional Phase of Boron Nitride: Few-Atomic-Layer Sheets and Suspended Membranes. *Appl. Phys. Lett.* **2008**, *92*, 1331071.
(23) Que, R. H.; Shao, M. W.; Wang, S. D.; Ma, D. D. D.; Lee, S. T. Silicon Nanowires with Permanent Electrostatic Charges for Nanogenerators. *Nano Lett.* **2011**, *11*, 4870−4873.
(24) Que, R. H.; Shao, Q.; Li, Q. L.; Shao, M. W.; Cai, S. D.; Wang, S. D.; Lee, S. T. Flexible Nanogenerators Based on Graphene Oxide Films for Acoustic Energy Harvesting. *Angew. Chem., Int. Ed.* **2012**, *51*, 5418−5422.
(25) Lei, W. W.; Portehault, D.; Dimova, R.; Antonietti, M. Boron Carbon Nitride Nanostructures from Salt Melts: Tunable Water-Soluble Phosphors. *J. Am. Chem. Soc.* **2011**, *133*, 7121−7127.

(26) Bengu, E.; Marks, L. D.; Ovali, R. V.; Gulseren, O. Analysis of Defects on BN Nano-Structures Using High-Resolution Electron Microscopy and Density-Functional Calculations. *Ultramicroscopy* **2008**, *108*, 1484−1489.
(27) Lin, Y.; Williams, T. V.; Cao, W.; Elsayed-Ali, H. E.; Connell, J. W. Defect Functionalization of Hexagonal Boron Nitride Nanosheets. *J. Phys. Chem. C* **2010**, *114*, 17434−17439.
(28) Song, L.; Ci, L. J.; Lu, H.; Sorokin, P. B.; Jin, C. H.; Ni, J.; Kvashnin, A. G.; Kvashnin, D. G.; Lou, J.; Yakobson, B. I.; Ajayan, P. M. Large Scale Growth and Characterization of Atomic Hexagonal Boron Nitride Layers. *Nano Lett.* **2010**, *10*, 3209−3215.
(29) Gorbachev, R. V.; Riaz, I.; Nair, R. R.; Jalil, R.; Britnell, L.; Belle, B. D.; Hill, E. W.; Novoselov, K. S.; Watanabe, K.; Taniguchi, T. Hunting for Monolayer Boron Nitride: Optical and Raman Signatures. *Small* **2011**, *7*, 465−468.
(30) Li, L. H.; Cervenka, J.; Watanabe, K.; Taniguchi, T.; Chen, Y. Strong Oxidation Resistance of Atomically Thin Boron Nitride Nanosheets. *ACS Nano* **2014**, *8*, 1457−1462.
(31) Komatsu, T.; Goto, A. Synthesis and Characterization of Graphite-like B−C−N Materials of Composition $CN_x(BN)_y$ ($x \ll 1$, $y \leq 1$). *J. Mater. Chem.* **2002**, *12*, 1288−1293.
(32) Liu, Y.; Zou, X.; Yakobson, B. I. Dislocation and Grain Boundaries in Two-Dimensional Boron Nitride. *ACS Nano* **2012**, *6*, 7053−7058.
(33) Roos, J. Electrets, Semipermanently Charged Capacitors. *J. Appl. Phys.* **1969**, *40*, 3135−3139.